Chemical Science

EDGE ARTICLE

Check for updates

The stability enhancement factor beyond eight-electron shell closure in thiacalix[4]arene-protected silver clusters†

Zong-Jie Guan,[ab] Feng Hu,[b] Shang-Fu Yuan,[ab] Zi-Ang Nan,[a] Yu-Mei Lin*[a] and Quan-Ming Wang ORCID *[ab]

We report the synthesis and structures of two 34-atom metal nanoclusters, namely $[Ag_{34}(BTCA)_3(C\equiv CBu^t)_9(tfa)_4(CH_3OH)_3]SbF_6$ and $[AuAg_{33}(BTCA)_3(C\equiv CBu^t)_9(tfa)_4(CH_3OH)_3]SbF_6$, where H_4BTCA is *p-tert*-butylthiacalix[4]arene and tfa is trifluoroacetate. Their compositions and structures have been determined by single-crystal X-ray structural analysis and ESI-MS. The cationic cluster consists of a centered icosahedron $M@Ag_{12}$ (M = Ag or Au) core that is surrounded by 21 peripheral silver atoms. Surrounding protection is provided by four kinds of ligands, including three BTCA, nine $^tBuC\equiv C$, four tfa, and three methanol solvent ligands. It was found that the $Ag_5@BTCA$ μ_5-coordination motif of thiacalixarene is critical for high stability of the title clusters, and extra stability enhancement can be achieved by doping a gold atom at the center of the silver cluster. This work suggests that coordination saturation should be taken into account in addition to electronic and geometric factors for analyzing metal nanocluster stabilities.
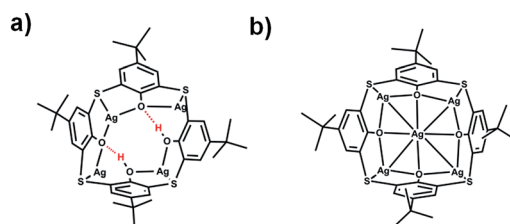
1 Introduction

Ligand-protected metal nanoclusters have attracted great attention owing to their structural diversity and potential application in catalysis, sensing, drug delivery, and bioimaging.[1–7] Various organic ligands as protecting agents have been used in the preparation of metal nanoclusters.[8–17] Among those coinage metal nanoclusters, some exhibit high thermodynamic and chemical stabilities, such as Au_{25},[9] Au_{38},[18] Au_{102},[8] Ag_{44},[14] $Au_{15}Ag_3$,[19] and $Au_{57}Ag_{53}$.[20] The stability of a cluster is important for its application in different fields. Many factors can affect the stability of a cluster, including electronic shell closing, geometric symmetry and metal doping.[14b,19,21–24] Moreover, it is noted that surface organic ligands also play a critical role in determining the stability,[25] atom packing,[26] and properties of metal clusters.[27] It has been found that the coordination preference, bulkiness, and electronic nature of ligands have significant effects on the structures and properties of the clusters.[17a,27,28]

Previously, we have demonstrated that macrocycle ligands such as thiacalixarene can be used in the protection of

*a*Department of Chemistry, College of Chemistry and Chemical Engineering, Xiamen University, Xiamen, 361005, PR China. E-mail: linyum@xmu.edu.cn; qmwang@xmu.edu.cn

*b*Department of Chemistry, Tsinghua University, Beijing, 100084, PR China

† Electronic supplementary information (ESI) available. CCDC 1863292 and 1863293. For ESI and crystallographic data in CIF or other electronic format see DOI: 10.1039/c8sc03756f

metal nanoclusters, because calixarenes have preorganized multidentate coordination sites.[29] We managed to isolate and determine the structure of $[Ag_{35}(H_2BTCA)_2(BTCA)(C\equiv CBu^t)_{16}]$-$(SbF_6)_3$ (H_4BTCA, *p-tert*-butylthiacalix[4]-arene) (denoted as **Ag_{35}**).[10g] While it was envisioned that calixarenes can enhance the stability of clusters by providing multisite protection, it turned out that the stability of the cluster **Ag_{35}** was not as good as expected. It decomposes in solution in one day, even though it is an eight-electron system and it is spherically shaped. In **Ag_{35}**, two types of coordination motifs of the thiacalixarene were observed, namely $Ag_4@H_2BTCA$ and $Ag_5@BTCA$ (see Scheme 1). One can see that there are two hydroxyl groups in $Ag_4@H_2BTCA$, and they interact with the other two phenoxyl oxygens to form intramolecular hydrogen bonds. We hypothesize that the poor stability of **Ag_{35}** is related to the $Ag_4@H_2BTCA$ motif, because it is not as rigid as $Ag_5@BTCA$. Moreover, the two protons may be labile in two ways: they may be removed when encountering a base; they

Scheme 1 Two types of coordination motifs: (a) $Ag_4@H_2BTCA$ and (b) $Ag_5@BTCA$.

may be replaced by other metal ions. Interestingly, we managed to prepare BTCA-protected silver nanoclusters containing no proton residues by adding excess silver salt Agtfa (tfa = trifluoroacetate) in the synthetic protocol and found that these nanoclusters bearing only Ag$_5$@BTCA motifs are much more stable than **Ag$_{35}$**.

Herein, we report the synthesis, total structure determination, optical properties, and electronic structure analysis of two metal nanoclusters protected by BTCA ligands: [Ag$_{34}$(BTCA)$_3$-(C≡CBu^t)$_9$(tfa)$_4$(CH$_3$OH)$_3$]SbF$_6$ (**1**) and [AuAg$_{33}$(BTCA)$_3$-(C≡CBu^t)$_9$(tfa)$_4$(CH$_3$OH)$_3$]SbF$_6$ (**2**). Cluster **2** is a single-gold-doped analogue of **1** and is isostructural to **1**.

2 Experimental

Materials

3,3-Dimethyl-1-butyne (^{t}BuC≡CH, 98%) and silver trifluoroacetate (Agtfa, 98%) were purchased from J&K; silver hexafluoroantimonate (AgSbF$_6$, 98.0%) and 4-*tert*-butylthiacalix[4]arene (H$_4$BTCA) were purchased from TCI; sodium borohydride (NaBH$_4$, 98%) and other reagents employed were purchased from Sinopharm Chemical Reagent Co. Ltd. (Shanghai, China). All reagents were used as received without further purification.

Synthesis of 1

To 2.0 mL CHCl$_3$ solution containing AgC≡CBu^t (0.1 mmol) and AgSbF$_6$ (0.1 mmol), 1.0 mL of methanol solution of Agtfa (0.06 mmol) was added, and then a freshly prepared solution of NaBH$_4$ (0.03 mmol in 1 mL of ethanol) was added dropwise under vigorous stirring. The solution color changed from colorless to pale brown and finally to dark brown. Then 3.0 mL CHCl$_3$ solution containing H$_4$BTCA (0.02 mmol) was added to the mixture, followed by addition of triethylamine (20 μL). Then the reaction continued for 3 h at room temperature in air in the dark. The mixture was evaporated to dryness to give a dark solid. This solid was dissolved in 8 mL *n*-hexane and centrifuged for 2 min at 9000 rpm, and then the supernatant was collected. The organic solvent was removed under rotary evaporation, and then the solid was dissolved in a mixture of diethyl ether (3 mL) and methanol (0.5 mL). After the solution was volatilized at 4 °C for about 7 days, sheet-like dark crystals deposited in 7% yield (3.8 mg, based on Ag).

Synthesis of 2

To 2.0 mL CHCl$_3$ mixture of AgC≡CBu^t (0.1 mmol) and AgSbF$_6$ (0.1 mmol), 1.0 mL methanol solution containing Agtfa (0.06 mmol) was added, and then a freshly prepared solution of NaBH$_4$ (0.03 mmol in 1 mL of ethanol) was added dropwise under vigorous stirring. The solution color changed from colorless to pale brown and finally to dark brown. Then 3.0 mL CHCl$_3$ solution containing H$_4$BTCA (0.02 mmol) was added to the mixture, followed by addition of triethylamine (20 μL). Finally, 1.0 mL CHCl$_3$ solution containing Me$_2$SAuCl (0.02 mmol) was added. Then the reaction continued for 3 h at room temperature in air in the dark. The mixture was evaporated to dryness to give a dark solid. This solid was dissolved in 8 mL *n*-hexane and centrifuged for 2 min at 9000 rpm, and then the

supernatant was collected. The organic solvent was removed under rotary evaporation, and then the solid was dissolved in a mixture of diethyl ether (3 mL) and methanol (0.5 mL). After the solution was volatilized at 4 °C for about 7 days, sheet-like dark crystals deposited in 10% yield (5.4 mg, based on Ag).

Characterization

UV-Vis-NIR absorption spectra were recorded on a Cary 5000. The mass spectrum was recorded on an ABI4800plus ESI-TOF-MS and Waters Q-TOF mass spectrometer. Intensity data of compounds **1** and **2** were collected on an Oxford Gemini S Ultra system (Cu K). Absorption corrections were applied by using the program CrysAlis (multi-scan). The structure was solved by direct methods, and C, O, S, F, Ag, Au atoms were refined anisotropically by least-squares on F^2 using the SHELXTL program. SbF$_6$$^-$ could not be located due to high symmetry, but the formula reported was confirmed by mass spectrometry (Fig. S1†). The diffuse electron densities resulting from the residual solvent molecules were removed from the data set using the SQUEEZE routine of PLATON.

Computational details

Density functional theory (DFT) calculations were performed with the quantum chemistry program Gaussian 09.[30] In the calculations, cluster **1** was mimicked by a model system of [Ag$_{34}$(TCA)$_3$(C≡CH)$_9$(tfa)$_4$]$^+$ and cluster **2** was mimicked by a model system of [AuAg$_{33}$(TCA)$_3$(C≡CH)$_9$(tfa)$_4$]$^+$. The 6-31G(d) basis set was used for C, H, O, S, F, and LANL2DZ for Ag and Au.[31] Geometry optimizations were performed with the B3LYP functional, and time-dependent DFT calculations of the UV-vis absorption spectrum were performed with the PBE functional.

3 Results and discussion

Single-crystal X-ray crystallography revealed that cluster **1** crystallized in the axisymmetric $R\bar{3}$ space group.[32] As shown in Fig. 1a, the monocationic cluster consists of 34 Ag atoms coordinated by four kinds of ligands, including three BTCA, nine ^{t}BuC≡C, four tfa, and three methanol ligands. The Ag$_{34}$ core has a centered icosahedron Ag@Ag$_{12}$ kernel that is surrounded by 21 peripheral silver atoms (Fig. 1b). As shown in Fig. 1c, all three calixarene ligands are in the same binding environment Ag$_5$@BTCA, and each of the calixarene ligands binds five silver atoms (one silver atom belongs to the icosahedral Ag$_{12}$ shell). This structural feature is different from the case of the reported **Ag$_{35}$** where there are two kinds of binding motifs (Ag$_4$@H$_2$BTCA and Ag$_5$@BTCA).[10g] Except for the 25 Ag atoms, the remaining nine silver atoms are surrounded by alkynyl, tfa and methanol ligands (Fig. 1d). In the Ag@Ag$_{12}$ core, the Ag⋯Ag distances between the central Ag atom and the Ag atoms of the Ag$_{12}$ shell have an average value of 2.779 Å, which is shorter than the average Ag⋯Ag distance within the Ag$_{12}$ shell (2.922 Å). These values are very close to those found in the Ag@Ag$_{12}$ core of **Ag$_{35}$** (2.778 and 2.923 Å, respectively).[10g] The average Ag⋯Ag distances from the 21 exterior Ag atoms to the Ag$_{12}$ shell are 3.03 Å. Alkynyl ligands adopt two types of
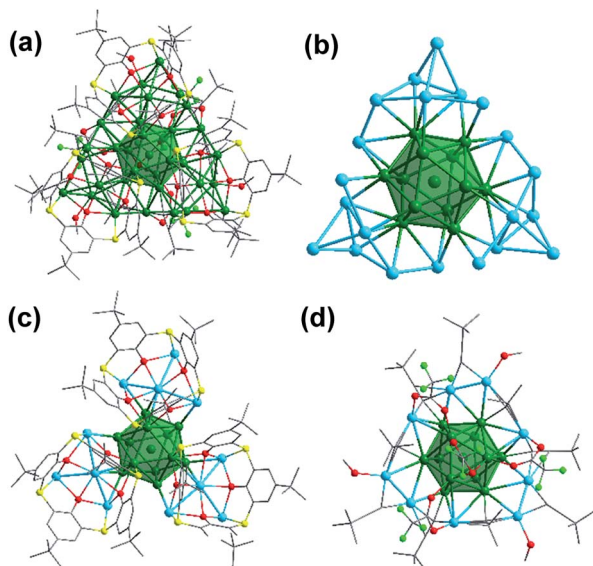
Fig. 1 (a) Molecular structure of **1**. (b) Ag_{34} kernel in **1**. (c) The additional 12 Ag atoms (sky blue) held by thiacalixarene ligands onto the $Ag@Ag_{12}$ core (green). (d) The 9 peripheral Ag atoms (sky blue) coordinated by alkynyl, tfa and MeOH ligands. Color legend: green, sky blue, silver; red, oxygen; yellow, sulfur; gray, carbon; bright green, fluorine. Hydrogen atoms were omitted for clarity.

coordination modes: three in μ_3-η^1,η^2,η^2 and six in μ_4-$\eta^1,\eta^1,\eta^2,\eta^2$ (Fig. S2†). Three tfa ligands employ a μ_2-η^1,η^1 mode, and the other tfa employs μ_3-η^1,η^1,η^1 mode (Fig. S3†). It's worth noting that there are three methanol molecules in the structure, which coordinate with the silver atoms with a Ag–O distance of 2.262 Å (Fig. 1d and S3†).

The composition of **1** was further confirmed by electrospray ionization mass spectrometry (ESI-MS) in positive mode, using CH_2Cl_2 as a solvent (Fig. 2). As shown in Fig. 2a, signals were observed at m/z = 3328.00, 3366.51, 3405.02, and 3444.01 corresponding to the molecular ions $[Ag_{34}(BTCA)_3(C\equiv CBu^t)_9Cl_3]^{2+}$,

$[Ag_{34}(BTCA)_3(C\equiv CBu^t)_9(tfa)Cl_2]^{2+}$, $[Ag_{34}(BTCA)_3(C\equiv CBu^t)_9(tfa)_2$-$Cl]^{2+}$, and $[Ag_{34}(BTCA)_3(C\equiv CBu^t)_9(tfa)_3]^{2+}$, respectively. Its isotopic distribution pattern is in perfect agreement with the simulated one (Fig. 2b, I and II). It was found that the tfa and methanol ligands can be removed under the conditions of the ESI-MS measurement.

Furthermore, doping effects were also studied by introducing a gold precursor in the synthesis, which resulted in the isolation of a mixed metal nanocluster, $[AuAg_{33}(BTCA)_3(-C\equiv CBu^t)_9(tfa)_4(CH_3OH)_3]SbF_6$ (**2**). X-ray crystal structure analysis revealed that **2** is isostructural to **1** (Fig. 3).[32] Cluster **2** can be derived from **1** by replacing the central Ag atom by a gold atom, *i.e.*, now it is a centered icosahedral $Au@Ag_{12}$ core instead of $Ag@Ag_{12}$. The Au⋯Ag distances from the central Au atom to the Ag_{12} shell have an average value of 2.780 Å, and the average bond length in the Ag_{12} shell is 2.923 Å. These values are almost the same as the Ag⋯Ag distances of $Ag@Ag_{12}$ in **1** (2.779 Å and 2.922 Å). It is worth noting that only a few examples of single-gold-doped Ag nanoclusters have been reported, such as $AuAg_{16}$,[33] $AuAg_{24}$,[34] $AuAg_{28}$,[35] and $AuAg_{19}$.[36]

Moreover, the composition of **2** was also verified by ESI-MS (Fig. S4†). One can see three intense peaks at m/z = 3411.05, 3450.06 and 3488.57, which can be assigned to $[AuAg_{33}(-BTCA)_3(C\equiv CBu^t)_9(tfa)Cl_2]^{2+}$, $[AuAg_{33}(BTCA)_3(C\equiv CBu^t)_9(tfa)_2$-$Cl]^{2+}$, and $[AuAg_{33}(BTCA)_3(C\equiv CBu^t)_9(tfa)_3]^{2+}$, respectively. A weak signal was found at m/z = 7186.13 corresponding to the molecular ion $[AuAg_{33}(BTCA)_3(C\equiv CBu^t)_9(tfa)_4(CH_3OH)_3]^+$. Its isotopic distribution pattern is in perfect agreement with the simulated one (Fig. S4†, III, IV, and V).

Clusters **1** and **2** give green solutions in CH_2Cl_2, and their absorption spectra are shown in Fig. 4. Cluster **1** shows three prominent absorption bands at 614, 457 and 339 nm. The two lower-energy absorption peaks were blue-shifted to 437 and 579 nm for **2**. To better understand the electronic structures of **1** and **2**, time-dependent density functional theory calculations were performed to investigate their frontier orbitals. As shown in Fig. S5a†, the absorption bands around 600 nm are attributed to the transitions from HOMO−2 to LUMO for cluster **1** and from HOMO−3 to LUMO for **2**. We found that the HOMO−2 of **1** and the HOMO−3 of **2** spread over the π orbital of the BTCA ligand, and their lowest unoccupied molecular orbitals are composed mainly of the orbitals of the metal core (Fig. S5†). Consequently, the lowest energy absorption peaks of the two clusters primarily come from the transition from thiacalixarene

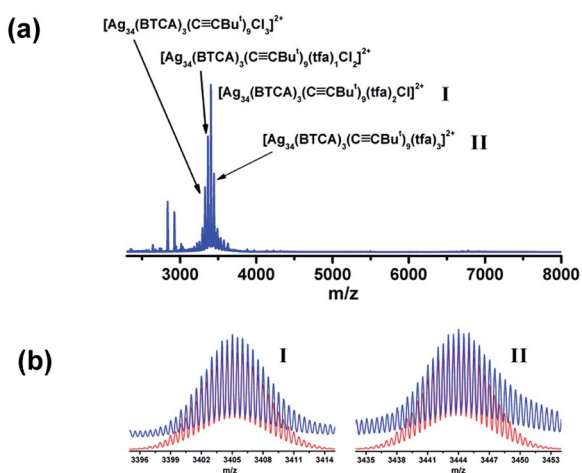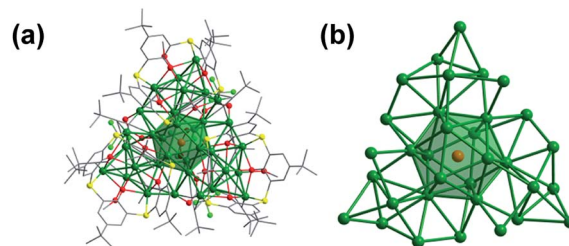**Fig. 2** (a) Mass spectrum of cluster **1**. (b) The measured (blue trace) and simulated (red trace) isotopic patterns of $[Ag_{34}(BTCA)_3(-C\equiv CBu^t)_9(tfa)_2Cl]^{2+}$ (I) and $[Ag_{34}(BTCA)_3(C\equiv CBu^t)_9(tfa)_3]^{2+}$ (II).

Fig. 3 (a) Molecular structure of **2**. (b) Metal core $AuAg_{33}$ in **2**. Color legend: green, silver; red, oxygen; yellow, sulfur; gray, carbon; bright green, fluorine. Hydrogen atoms were omitted for clarity.
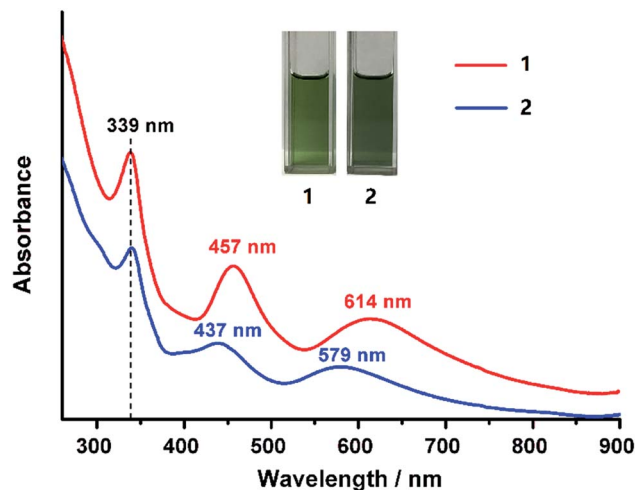
Fig. 4 The optical absorption spectra of $[Ag_{34}(BTCA)_3(C{\equiv}CBu^t)_9(tfa)_4(CH_3OH)_3](SbF_6)$ (**1**) and $[AuAg_{33}(BTCA)_3(C{\equiv}CBu^t)_9(tfa)_4(CH_3OH)_3](SbF_6)$ (**2**) in dichloromethane solution. Inset: photographs of cluster solutions.

to metal kernel. Theoretical studies revealed that **1** and **2** have similar frontier orbitals, but the HOMO–LUMO gap of **2** is slightly larger than that of **1** (Fig. S6†). However, the higher-energy absorption peaks at 339 nm for **1** and **2** are the same, indicating that the central metal does not make any contribution, and are probably associated with the surface $Ag_5@BTCA$ motifs. It is worth noting that the peak at 339 nm for **1** is also similar to that of Ag_{35}, although their absorption peaks at 400 to 650 nm are different.[10g] Nevertheless, the 339 nm peak of cluster **1** is sharper than that of Ag_{35}, which indicated that this peak is related to the coordination motifs of thiacalixarene.

Clusters **1**, **2** and Ag_{35} have very similar geometric structures, and all of them are 8-electron systems, so they are supposed to have similar stability. To our surprise, in contrast to the poor stability of Ag_{35}, **1** and **2** are much more stable as monitored by UV-vis spectroscopy. No decomposition was observed after the solutions of **1** and **2** had been stored under ambient conditions for at least three weeks in the absence of light (Fig. 5a and b), while Ag_{35} was only stable for less than one day under the same conditions (Fig. 5c). The $Ag_4@H_2BTCA$ motif in Ag_{35} may account for its instability (Fig. S7†). Compared with the rigid $Ag_5@BTCA$ motif in **1** and **2**, $Ag_4@H_2BTCA$ is distorted and it contains two labile hydroxyl hydrogens, which allows for the coordination of silver ions. As shown in Fig. 5c, the peak at 336 nm became sharp as Ag_{35} was stored for one day, which indicated that $Ag_4@H_2BTCA$ was converted to $Ag_5@BTCA$ through binding an additional silver atom. Thus, Ag_{35} decomposed as a result of binding silver ions generated from other Ag_{35}. In contrast, there is only one type of coordination motif of thiacalixarene with silver atoms in **1** and **2**, $Ag_5@BTCA$. As the coordination of BTCA is saturated, no transformation from $Ag_4@H_2BTCA$ to $Ag_5@BTCA$ is possible. In addition, three rigid $Ag_5@BTCA$ motifs in **1** or **2** will strengthen the interactions between the metal kernel and the ligands. Consequently, two title clusters are much more stable than Ag_{35}. It is noted that
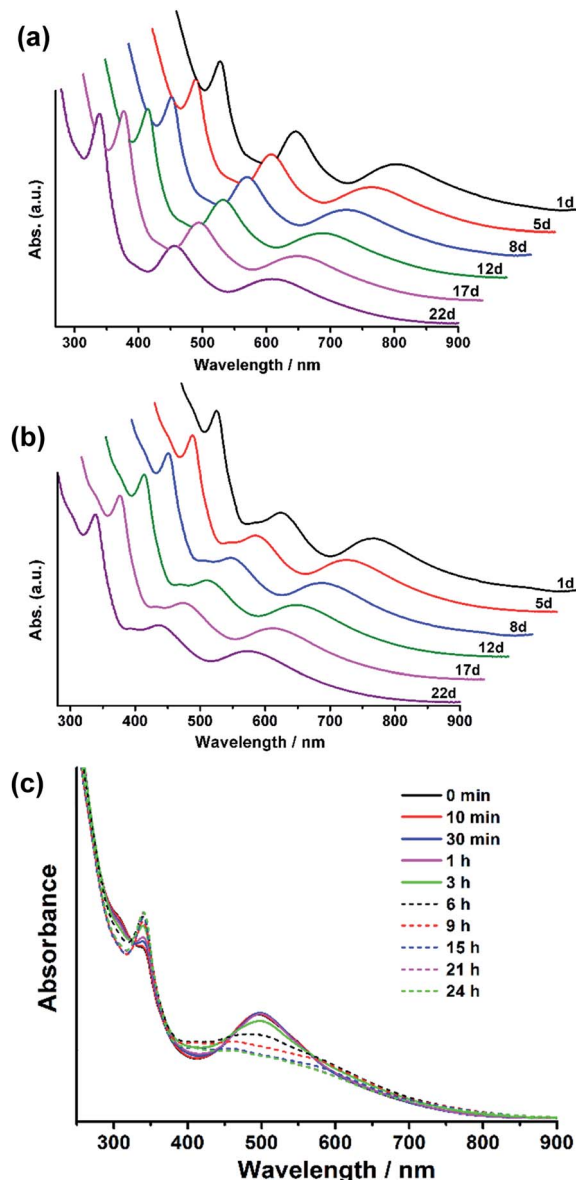

Fig. 5 (a) Time dependences of absorption spectra of **1** in CH_2Cl_2. (b) Time dependences of absorption spectra of **2** in CH_2Cl_2. (c) Time dependences of absorption spectra of Ag_{35} in CH_2Cl_2.

previous studies have underscored the role of coordinating species in the stability of silver clusters.[14a,33,37] Bigioni and coworkers found that the coordinating solvent can plug up the hole of the ligand shell to stabilize the nanoclusters, though no direct structural evidence was available.[37] In this study, the effect of coordinating species was confirmed by single crystal structure determination.

Interestingly, cluster **2** exhibits higher stability than **1** in solution under ambient conditions. As shown in Fig. S8†, the optical absorption spectrum of **2** remained unchanged for at least 21 days. However, the absorption peaks at 457 nm and 614 nm for **1** were significantly attenuated after 10 days. This observation indicates that doping of **1** with one Au atom forms a more stable cluster **2**. Note that similar cases have been

observed in $Ag_{29-x}Au_x(BDT)_{12}(TPP)_4$,[35] $M_4Au_xAg_{44-x}(SR)_{30}$,[14b,38] $PdAu_{24}(SR)_{18}$ and $Pd_2Au_{36}(SC_2H_4Ph)_{24}$.[24,39] Teo *et al.* developed the strong-bond rule and heterobond rule to explain the stability enhancement of doped clusters. These empirical rules are also applicable in explaining the stability difference between **1** and **2**. Doping a single Au atom in a Ag nanocluster leads to stronger metal–metal bonds, *i.e.* the bond energy of Au–Ag is greater than that of Ag–Ag in the present case, and the number of heterobonds is maximized as the Au atom is located at the center of the Ag_{12} icosahedron.[40,41] Our theoretical calculation also demonstrates that the interaction energy between the central atom and the Ag_{12} shell in **2** is larger than that in **1** (Table S1†). In addition, electrophilicity of gold atoms is also accountable for the stabilization of heteronuclear nanoclusters.[38]

Overall, the stability difference between **1** and **2** is thermodynamic in nature, while the dynamic factor plays a critical role, resulting in the stability enhancement from **Ag₃₅** to **1**.

4 Conclusion

Previous studies have emphasized that electronic shell closing and geometric symmetry are two important factors for nanocluster stability,[21–23] and this work further indicates that the extent of coordination saturation of ligands is also critical for the stability of metal nanoclusters. The reactivity of a nanocluster with unsaturated coordination sites could be lowered through adding metal ions such as Ag^+ to achieve coordination saturation in the present case. While an 8-electron shell closure has been identified as an important factor accounting for the stability of many metal nanoclusters, poor stability was still found in 8e system **Ag₃₅**. These findings suggest that coordination saturation should be taken into account in addition to electronic and geometric factors for analyzing nanocluster stabilities.

Conflicts of interest

There are no conflicts to declare.

Acknowledgements

Notes and references

1 M. C. Daniel and D. Astruc, *Chem. Rev.*, 2004, **104**, 293–346.

2 R. Jin, C. Zeng, M. Zhou and Y. Chen, *Chem. Rev.*, 2016, **116**, 10346–10413.

3 J. F. Parker, C. A. Fields-Zinna and R. W. Murray, *Acc. Chem. Res.*, 2010, **43**, 1289–1296.

4 G. Schmid, *Chem. Soc. Rev.*, 2008, **37**, 1909–1930.

5 R. X. Jin, S. Zhao, Y. Xing and R. Jin, *CrystEngComm*, 2016, **18**, 3996–4005.

6 Z. Lei, X.-K. Wan, S.-F. Yuan, J.-Q. Wang and Q.-M. Wang, *Dalton Trans.*, 2017, **46**, 3427–3434.

7 S. Yamazoe, K. Koyasu and T. Tsukuda, *Acc. Chem. Res.*, 2014, **47**, 816–824.

8 P. D. Jadzinsky, G. Calero, C. J. Ackerson, D. A. Bushnell and R. D. Kornberg, *Science*, 2007, **318**, 430–433.

9 (a) M. Zhu, C. M. Aikens, F. J. Hollander, G. C. Schatz and R. Jin, *J. Am. Chem. Soc.*, 2008, **130**, 5883–5885; (b) M. W. Heaven, A. Dass, P. S. White, K. M. Holt and R. W. Murray, *J. Am. Chem. Soc.*, 2008, **130**, 3754–3755.

10 (a) X.-K. Wan, Q. Tang, S.-F. Yuan, D.-e. Jiang and Q.-M. Wang, *J. Am. Chem. Soc.*, 2015, **137**, 652–655; (b) X.-K. Wan, S.-F. Yuan, Z.-W. Lin and Q.-M. Wang, *Angew. Chem., Int. Ed.*, 2014, **53**, 2923–2926; (c) X.-K. Wan, S.-F. Yuan, Q. Tang, D.-e. Jiang and Q.-M. Wang, *Angew. Chem., Int. Ed.*, 2015, **54**, 5977–5980; (d) X.-K. Wan, W.-W. Xu, S.-F. Yuan, Y. Gao, X.-C. Zeng and Q.-M. Wang, *Angew. Chem., Int. Ed.*, 2015, **54**, 9683–9686; (e) X.-K. Wan, Z.-W. Lin and Q.-M. Wang, *J. Am. Chem. Soc.*, 2012, **134**, 14750–14752; (f) J.-L. Zeng, Z.-J. Guan, Y. Du, Z.-A. Nan, Y.-M. Lin and Q.-M. Wang, *J. Am. Chem. Soc.*, 2016, **138**, 7848–7851; (g) Z.-J. Guan, J.-L. Zeng, Z.-A. Nan, X.-K. Wan, Y.-M. Lin and Q.-M. Wang, *Sci. Adv.*, 2016, **2**, e1600323.

11 Z. Gan, J. Chen, J. Wang, C. Wang, M. B. Li, C. Yao, S. Zhuang, A. Xu, L. Li and Z. Wu, *Nat. Commun.*, 2017, **8**, 14739.

12 (a) Y. Chen, C. Zeng, C. Liu, K. Kirschbaum, C. Gayathri, R. R. Gil, N. L. Rosi and R. Jin, *J. Am. Chem. Soc.*, 2015, **137**, 10076–10079; (b) C. Zeng, Y. Chen, K. Kirschbaum, K. Appavoo, M. Y. Sfeir and R. Jin, *Sci. Adv.*, 2015, **1**, e1500045; (c) C. Zeng, Y. Chen, K. Kirschbaum, K. J. Lambright and R. Jin, *Science*, 2016, **354**, 1580–1584.

13 (a) S. Wang, S. Jin, S. Yang, S. Chen, Y. Song, J. Zhang and M. Zhu, *Sci. Adv.*, 2015, **1**, e1500441; (b) W. Du, S. Jin, L. Xiong, M. Chen, J. Zhang, X. Zou, Y. Pei, S. Wang and M. Zhu, *J. Am. Chem. Soc.*, 2017, **139**, 1618–1624.

14 (a) A. Desireddy, B. E. Conn, J. Guo, B. Yoon, R. N. Barnett, B. M. Monahan, K. Kirschbaum, W. P. Griffith, R. L. Whetten, U. Landman and T. P. Bigioni, *Nature*, 2013, **501**, 399–402; (b) H. Yang, Y. Wang, H. Huang, L. Gell, L. Lehtovaara, S. Malola, H. Hakkinen and N. Zheng, *Nat. Commun.*, 2013, **4**, 2422.

15 (a) H. Yang, Y. Wang, X. Chen, X. Zhao, L. Gu, H. Huang, J. Yan, C. Xu, G. Li, J. Wu, A. J. Edwards, B. Dittrich, Z. Tang, D. Wang, L. Lehtovaara, H. Hakkinen and N. Zheng, *Nat. Commun.*, 2016, **7**, 12809; (b) Y. Wang, X.-K. Wan, L. Ren, H. Su, G. Li, S. Malola, S. Lin, Z. Tang, H. Hakkinen, B. K. Teo, Q.-M. Wang and N. Zheng, *J. Am. Chem. Soc.*, 2016, **138**, 3278–3281; (c) H. Yang, J. Yan, Y. Wang, H. Su, L. Gell, X. Zhao, C. Xu, B. K. Teo, H. Hakkinen and N. Zheng, *J. Am. Chem. Soc.*, 2017, **139**, 31–34.

16 R. S. Dhayal, J. H. Liao, Y. C. Liu, M. H. Chiang, S. Kahlal, J. Y. Saillard and C. W. Liu, *Angew. Chem., Int. Ed.*, 2015, **54**, 3702–3706.

17 (a) C. P. Joshi, M. S. Bootharaju, M. J. Alhilaly and O. M. Bakr, *J. Am. Chem. Soc.*, 2015, **137**, 11578–11581; (b) M. J. Alhilaly, M. S. Bootharaju, C. P. Joshi, T. M. Besong, A. H. Emwas, R. Juarez-Mosqueda, S. Kaappa, S. Malola, K. Adil,

A. Shkurenko, H. Hakkinen, M. Eddaoudi and O. M. Bakr, *J. Am. Chem. Soc.*, 2016, **138**, 14727–14732; (*c*) M. S. Bootharaju, S. M. Kozlov, Z. Cao, M. Harb, N. Maity, A. Shkurenko, M. R. Parida, M. N. Hedhili, M. Eddaoudi, O. F. Mohammed, O. M. Bakr, L. Cavallo and J. M. Basset, *J. Am. Chem. Soc.*, 2017, **139**, 1053–1056.

18 H. Qian, W. T. Eckenhoff, Y. Zhu, T. Pintauer and R. Jin, *J. Am. Chem. Soc.*, 2010, **132**, 8280–8281.

19 (*a*) J. Xiang, P. Li, Y. Song, X. Liu, H. Chong, S. Jin, Y. Pei, X. Yuan and M. Zhu, *Nanoscale*, 2015, **7**, 18278–18283; (*b*) M. Zhu, X. Kang, C. Silalai, Y. Lv, G. Sun, S. Chen, H. Yu and F. Xu, *Eur. J. Inorg. Chem.*, 2017, 1414–1419.

20 Z.-J. Guan, J.-L. Zeng, S.-F. Yuan, F. Hu, Y.-M. Lin and Q.-M. Wang, *Angew. Chem., Int. Ed.*, 2018, **57**, 5703–5707.

21 M. Walter, J. Akola, O. Lopez-Acevedo, P. D. Jadzinsky, G. Calero, C. J. Ackerson, R. L. Whetten, H. Gronbeck and H. Hakkinen, *Proc. Natl. Acad. Sci. U. S. A.*, 2008, **105**, 9157–9162.

22 T. Higaki, C. Liu, M. Zhou, T. Y. Luo, N. L. Rosi and R. Jin, *J. Am. Chem. Soc.*, 2017, **139**, 9994–10001.

23 Y. Negishi, C. Sakamoto, T. Ohyama and T. Tsukuda, *J. Phys. Chem. Lett.*, 2012, **3**, 1624–1628.

24 Y. Negishi, K. Igarashi, K. Munakata, W. Ohgake and K. Nobusada, *Chem. Commun.*, 2012, **48**, 660–662.

25 (*a*) S. Kumar and R. Jin, *Nanoscale*, 2012, **4**, 4222–4227; (*b*) W. Kurashige, M. Yamaguchi, K. Nobusada and Y. Negishi, *J. Phys. Chem. Lett.*, 2012, **3**, 2649–2652.

26 Y. Chen, C. Zeng, D. R. Kauffman and R. Jin, *Nano Lett.*, 2015, **15**, 3603–3609.

27 (*a*) X.-K. Wan, J.-Q. Wang, Z.-A. Nan and Q.-M. Wang, *Sci. Adv.*, 2017, **3**, e1701823; (*b*) X.-K. Wan, Z.-J. Guan and Q.-M. Wang, *Angew. Chem., Int. Ed.*, 2017, **56**, 11494–11497.

28 Y. Song, S. Wang, J. Zhang, X. Kang, S. Chen, P. Li, H. Sheng and M. Zhu, *J. Am. Chem. Soc.*, 2014, **136**, 2963–2965.

29 Y. Bi, S. Du and W. Liao, *Coord. Chem. Rev.*, 2014, **276**, 61–72.

30 M. J. Frisch, *et al.*, *Gaussian 09, Revision A.1*, Wallingford, CT, 2009.

31 (*a*) A. D. Becke, *Phys. Rev. A: At., Mol., Opt. Phys.*, 1988, **38**, 3098–3100; (*b*) P. J. Hay and W. R. Wadt, *J. Chem. Phys.*, 1985, **82**, 299–310.

32 Crystal data for $C_{185}H_{225}Ag_{34}F_{12}O_{23}S_{12}$: $a = 22.3399(15)$, $b = 22.3399(15)$, $c = 94.097(4)$ Å, $\alpha = 90°$, $\beta = 90°$, $\gamma = 120°$, $V = 40\ 670(7)$ Å^3, space group $R\bar{3}$, $Z = 6$, $T = 100$ K, 41 087 reflections measured, 13 425 unique ($R_{int} = 0.1077$), $R_1 = 0.1228$ and $wR_2 = 0.3583$ for 7537 observed reflections [$I > 2\sigma(I)$]. Crystal data for $C_{185}H_{225}Ag_{33}AuF_{12}O_{23}S_{12}$: $a = 22.3959(16)$, $b = 22.3959(16)$, $c = 94.475(7)$ Å, $\alpha = 90°$, $\beta = 90°$, $\gamma = 120°$, $V = 41\ 038(8)$ Å^3, space group $R\bar{3}$, $Z = 6$, $T = 100$ K, 25 371 reflections measured, 14 044 unique ($R_{int} = 0.0937$), $R_1 = 0.0971$ and $wR_2 = 0.2840$ for 8427 observed reflections [$I > 2\sigma(I)$].

33 B. E. Conn, A. Atnagulov, B. Yoon, R. N. Barnett, U. Landman and T. P. Bigioni, *Sci. Adv.*, 2016, **2**, e1601609.

34 M. S. Bootharaju, C. P. Joshi, M. R. Parida, O. F. Mohammed and O. M. Bakr, *Angew. Chem., Int. Ed.*, 2016, **55**, 922–926.

35 G. Soldan, M. A. Aljuhani, M. S. Bootharaju, L. G. AbdulHalim, M. R. Parida, A. H. Emwas, O. F. Mohammed and O. M. Bakr, *Angew. Chem., Int. Ed.*, 2016, **55**, 5749–5753.

36 Y.-R. Lin, P. V. V. N. Kishore, J.-H. Liao, S. Kahlal, Y.-C. Liu, M.-H. Chiang, J.-Y. Saillard and C. W. Liu, *Nanoscale*, 2018, **10**, 6855–6860.

37 B. E. Conn, A. Desireddy, A. Atnagulov, S. Wickramasinghe, B. Bhattarai, B. Yoon, R. N. Barnett, Y. Abdollahian, Y. W. Kim, W. P. Griffith, S. R. J. Oliver, U. Landman and T. P. Bigioni, *J. Phys. Chem. C*, 2015, **119**, 11238–11249.

38 B. E. Conn, A. Atnagulov, B. Bhattarai, B. Yoon, U. Landman and T. P. Bigioni, *J. Phys. Chem. C*, 2018, **122**, 13166–13174.

39 (*a*) Y. Negishi, W. Kurashige, Y. Niihori, T. Iwasa and K. Nobusada, *Phys. Chem. Chem. Phys.*, 2010, **12**, 6219–6225; (*b*) D.-e. Jiang and S. Dai, *Inorg. Chem.*, 2009, **48**, 2720–2722.

40 B. K. Teo and A. Strizhev, *Inorg. Chem.*, 2002, **41**, 6332–6342.

41 B. K. Teo and H. Zhang, *Coord. Chem. Rev.*, 1995, **143**, 611–636.